2003

ENTRAINMENT OF ELECTRICAL ACTIVATION BY SPATIO-TEMPORAL DISTRIBUTED PACING DURING VENTRICULAR FIBRILLATION

Yiping Gu
University of Kentucky, ygu2@uky.edu

ABSTRACT OF THESIS

ENTRAINMENT OF ELECTRICAL ACTIVATION BY SPATIO-TEMPORAL DISTRIBUTED PACING DURING VENTRICULAR FIBRILLATION

Spatio-temporal variation in action intervals during ventricular fibrillation (VF) suggest that the excitable gap may also be distributed spatio-temporally. The observation lead us to hypothesize that distributed pacing can be used to modify and entrain electrical activation during VF. We tested this hypothesis using simulated VF and animal studies.

We simulated VF in a 400 by 400 cell matrix. Simulation results showed that activation pattern could be entrained using spatially distributed stimulation. Up to a certain limit, increasing stimulus strength and density led to improved entrainment. Best entrainment was obtained by pacing at a cycle length similar to the intrinsic cycle length.

In order to verify whether activation could be entrained experimentally, eight optically isolated biphasic TTL addressable stimulators were fabricated. Distributed stimulation was tested during electrically induced VF in two canines and two swine. Results showed that electrical activation could be entrained in both species. Similar to that in simulation, better entrainment was obtained with denser pacing distribution and at pacing cycle length similar to the intrinsic cycle length. As expected, entrainment was affected by tissue thickness. Our results show that spatio-temporally distributed pacing strength stimuli can be used to modify activation patterns during VF.

KEYWORDS: Ventricular Fibrillation (VF), Defibrillation, Simulation, Pacing, Entrainment of Activation

Yiping Gu

April, 2003

ENTRAINMENT OF ELECTRICAL ACTIVATION BY SPATIO-TEMPORAL DISTRIBUTED PACING DURING VENTRICULAR FIBRILLATION

By

Yiping Gu

Dr. Abhijit Patwardhan
(Director of Thesis)

Dr. David Puleo
(Director of Graduate Studies)

April, 2003

RULES FOR THE USE OF THESES

Unpublished theses submitted for the Master's degree and deposited in the University of Kentucky Library are as a rule open for inspection, but are to be used only with due regard to the rights of the authors. Bibliographical references may be noted, but quotations or summaries of parts may be published only with the permission of the author, and with the usual scholarly acknowledgements.

Extensive copying or publication of the thesis in whole or in part also requires the consent of the Dean of the Graduate School of the University of Kentucky

Name Date

_____

_____

_____

_____

_____

_____

THESIS

Yiping Gu

The Graduate School

University of Kentucky

2003

ENTRAINMENT OF ELECTRICAL ACTIVATION BY SPATIO-TEMPORAL DISTRIBUTED PACING DURING VENTRICULAR FIBRILLATION

THESIS

A thesis submitted in partial fulfillment of the
requirements for the degree of Master of Science in
Biomedical Engineering
at the University of Kentucky

By
Yiping Gu
Lexington, Kentucky
Director: Dr. Abhijit Patwardhan, Associate Professor
Center for Biomedical Engineering
Lexington, Kentucky
2003

TABLE OF CONTENTS

List of Tables

List of Figures

List of Files

GuThesis.pdf	861k
Video1.avi	78.9M

Chapter One : Introduction

1.1 Background

1.1.1 Sudden Cardiac Death

Most sudden cardiac death occurs when the heart's electrical activity becomes rapid (ventricular tachycardia) and then unsynchronized (ventricular fibrillation). The common underlying reason for sudden cardiac death is coronary heart disease (CHD) (1). Although no statistics of cardiac arrests are available, about 250,000 Americans died of CHD without diagnosis every year (1, 2).

1.1.2 Ventricular Fibrillation and Defibrillation

Ventricular fibrillation (VF) is defined as the disruption of heart's electrical activity. During VF, synchronous ventricular contraction is lost, and little or no blood is pumped out when this happens (1). Irreversible damage happens to the heart and brain if circulation is not restored within a few minutes following the onset of VF.

Drugs that are currently available (e.g. Sotalol (3) or Amiodarone HCL (4)) can only lower the probability of the occurrence of VF but cannot stop it. Once VF occurs, the most effective, and perhaps the only way to terminate it is defibrillation, delivery of an electrical shock across the heart or the thorax. An implantable defibrillator is the best available therapy for individuals at high risk for sudden cardiac death. External defibrillation therapy has been available for 30 years and there have been many improvements, but the mechanism of defibrillation is still unknown.

The efficacy of a defibrillator is strongly dependent on the defibrillation threshold of the tissue, the energy required to disrupt reentrant wavefront. In practice, the implantable defibrillators deliver a sufficiently high energy shock to the heart to provide enough safety margin, that is the shock is of much larger amplitude than the defibrillation threshold. But high energy shocks also cause considerable myocardial damage and change the electrophysiological properties of the myocardium (5,25). It is important, therefore, to find a way to reduce defibrillation shock energies while still successfully defibrillating the heart.

1.1.3 Existence of Excitable Gap during Ventricular Fibrillation

The mechanisms of VF remain unclear after extensive epicardial and optical studies. Previous studies have suggested that during VF, the myocardium is excited by a reentrant wavefront as soon as it recovers from the absolute refractory period (6), i.e. there is no excitable gap. An excitable gap is defined as time after end of the absolute refractory period and during which a stimulus can produce a propagated action potential. However, KenKnight et al. (7), using epicardial unipolar electrograms, showed that it was possible to obtain capture during VF in an area close to a stimulating electrode delivering bipolar pacing stimuli. The possible explanation for these somewhat discrepant observations is that an excitable gap exists during VF and the myocardium can be excited by use of pacing strength. The existence of an excitable gap leads to hypothesis that it may be possible to entrain electrical activation during VF.

1.2 Rationale for the Study

The outcome of a defibrillation shock is a statistical phenomenon (16). Even if shocks are delivered at the same energy, voltage, current and resistance, some shocks can terminate VF, while others cannot. The probabilistic nature of defibrillation indicates that there may be some intrinsic properties of the tissue, like the random variance in conductive properties and electrophysiological characteristics, correlated with the outcome of the defibrillation shocks. Jones et al. (8) reported that the successful rate of defibrillation was improved if the shock was synchronized according to the action potential in low-gradient regions before defibrillation. Locally propagated activation sometimes blocked globally propagated activation after the shocks (26). In a previous study, it was observed that the successful rate of defibrillation shock was higher when it was delivered at more synchronized activation (9).

Evidence from the above studies indicates that the spatial distribution of electrical activation in low-gradient regions before defibrillation has important affects on the outcome of defibrillation shocks. Therefore, we and others (18) hypothesize that defibrillation threshold may be reduced if the activation pattern in low-gradient regions

becomes uniform before defibrillation. Excitable gaps exist during VF; therefore, the fibrillating tissue could be excited by the pacing strength stimuli, modifying the activation into a more uniform pattern. The principal aim of this study is to demonstrated that it is possible to entrain the activation and modify it into a uniform pattern during VF by the use of spatio-temporal distributed stimuli.

1.3 Objectives of the Study

The first objective of the study was to develop hardware and software to deliver spatio-temporal distributed stimuli and to verify the entrainment of activation during VF. The second objective was to elucidate the parameters that might influence the entrainment, such as stimuli strength, stimuli density, and pacing cycle length. Studies were based on in-vivo experiments and simulated VF. The simulations use a Luo-Rudy ionic model for transmembrane ionic currents (12, 13, 14).

Chapter Two : Methods

2.1 Numerical Model of Cardiac Activation and Simulation of VF

To aid the design of pacing protocol and investigate the mechanism of entrainment, a mathematical model was used to simulate the activation of a single layer of cells during VF.

2.1.1 Model of a Single Cell

A Luo-Rudy (L-R) model is a detailed ionic current model, which includes six different ionic currents (12). A brief description of the model is given below. The rate of change of membrane potential is given by

$$\frac{dV}{dt} = -(\frac{1}{C})(I_i + I_{st}) \qquad Eq.\ 2.1$$

where V is the membrane potential, C is the membrane capacitance, I_{st} is stimulus current, and I_i is the sum of six ionic currents:

Fast sodium current: $I_{Na} = G_{Na} \cdot m^3 \cdot h \cdot j(V - E_{Na})$;

Slow inward current: $I_{si} = G_{si} \cdot d \cdot f \cdot (V - E_{si})$;

Time-dependent potassium current: $I_K = \overline{G_K} \cdot X \cdot X_i \cdot (V - E_K)$;

Time-independent potassium current: $I_{KI} = \overline{G_{KI}} \cdot KI_x \cdot (V - E_{KI})$;

Plateau potassium current: $I_{Kp} = 0.0183 \cdot Kp \cdot (V - E_{Kp})$;

Time-independent background current: $I_b = 0.03921 \cdot (V + 59.87)$.

The gate variables are $m, h, j, d, f,$ and X; and G_x is the maximum conductance of the ion channel x. The ionic currents are determined by the state of ionic gates. The properties of ionic gates are given by gating variables, which are the solutions of eight nonlinear ordinary differential equations in a coupled system. The ionic currents, in turn, change V, which subsequently affects the ionic gates and currents. (12)

The original L-R model reconstructs the action potential duration (APD) at about 360 msec. To simulate the real APD in canines and swine, we fixed $G_{Na} = 16mS/cm^2$ similar to that given in the later Luo-Rudy dynamic model (13,14).

2.1.2 Model of One Layer Cells

A homogeneous 400×400-cell matrix was simulated. The reaction-diffusion-like equation (equation 2.2) was used to describe the conduction between cells (analogous to gap junctions in real cardiac tissue)(15).

$$\frac{\partial V}{\partial t} = -\frac{(I_{ion} + I_{st})}{C} + \nabla \bullet (D\nabla V) \qquad Eq.\ \ 2.2$$

V, C, I_{ion}, and I_{st} have the same definition as equation 2.1 and D is the diffusion tensor with the structure: $D = \begin{bmatrix} D_{xx} & D_{xy} \\ D_{yx} & D_{yy} \end{bmatrix}$. Based on the assumption of homogeneity and no diffusion in the diagonal direction, D_{xx} equals D_{yy}, and D_{xy} and D_{yx} both equal zero. A cylindrical boundary condition on two sides of the matrix and zero flux condition on the other two sides was used in our simulation.

2.1.3 Numerical Methods Used in Simulation

Operator splitting and adaptive time step methods were implemented to integrate the ordinary differential equations and the partial differential equations in the model (15). The minimum time step was 0.01 msec, and the maximum time step was 0.2 msec for ordinary differential equations. Partial differential equations were integrated at every 0.2msec. Details of the numerical integration scheme are given in reference 15. Ventricular fibrillation was initiated in the simulation by the use of cross S1-S2 stimulation.

2.1.4 Methods to Analyze the Simulation Results

Two methods were used to evaluate the simulation results; animated display and numerical quantification. The transmembrane voltage was displayed as isopotential plots in color scale (details in result part). The action potential duration (APD) was measure at different simulation elements. Entrainment of one element was defined as

APD of two consecutive cycles is the same as the stimulation cycle length at that time. The obvious advantage of animated display is that we can get a direct impression of the activation propagation to tell whether capture is achieved or not. However, we cannot get quantitative measures of entrainment by animation. We calculated the activation interval on different sites by differentiating the transmembrane voltage (equation 2.1). By comparing the activation interval with the pacing cycle length, we could determine the duration of entrainment in simulation.

2.2 Animal Preparation

Data were collected from two swine and two canines. Animals were premedicated with an intramuscular injection of ketamine (20 mg/kg) and acepromazine (1mg/kg) (in case of swine) and then anesthetized with intravenous sodium pentobarbital (40 mg/kg). All animals were intubated, and ventilated with room air supplemented with oxygen. A carotid artery was cannulated to monitor blood pressure and a jugular vein was cannulated to administer fluids. The heart was exposed via a median sternotomy. A patch (Figure 2.1) with 121 recording electrodes (circles) and 64 stimulating electrodes (stars) was placed over the right ventricle free wall.

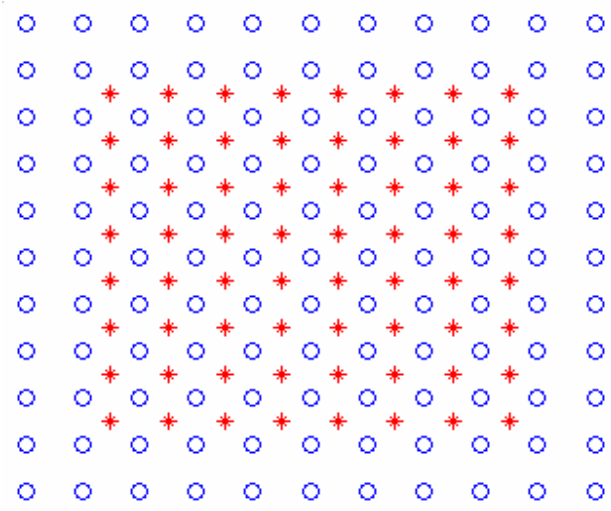

Figure 2.1 Patch electrodes include 121 recording electrodes (circle)and 64 pacing electrodes (star).

The patch location was approximately midway between the apex and the base with one wall of the patch parallel to the left anterior descending artery (LAD). The stimulation electrodes in each row were connected together as one line electrode. A defibrillation lead was introduced from the jugular vein and placed at the right ventricular apex. A sub-dermal patch electrode was sewn onto the left chest wall. Induction of VF was achieved by sending a high frequency burst shock (15V, 30Hz) through the third line of stimulating electrodes for 3 seconds. The pacing protocol was started after 5 seconds of VF. Epicardium electrograms were recorded for 35 seconds (Figure 2.2). As soon as the mechanical relay switches (described in section 2.2) were opened to protect the A/D converters, defibrillation shocks were delivered through the lead at the right ventricular apex and the patch electrodes.

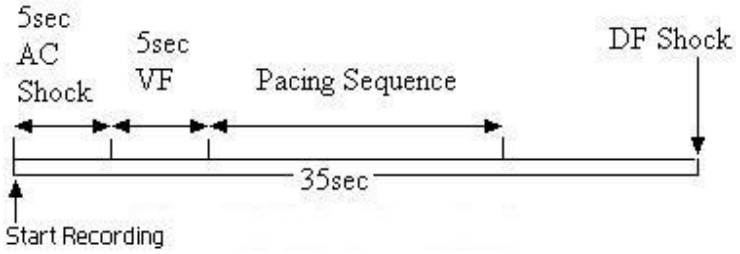

Figure 2.2 Timing of recording part in one trial. At least 10 minutes were allowed to resolve ischemia after recording

At least 10 minutes were allowed between trials to resolve ischemia.

2.3 System Scheme

Figure 2.3 shows the setup for the study. The starting point of recording of electrograms from the recording electrodes shown in Figure 2.2 was determined by a digital signal from computer 1. A custom written timing program running on computer 1 controlled the timing of the stimulators according to different pacing protocols and synchronized the entire system shown in Figure 2.3. The program started the analog to digital (A/D) converters housed in computer 2 after the 128 channel relay switches were closed. The code also delivered defibrillator shocks after opening the relay switches 20 msec before the shock and closed the relay switches 15 msec after the shock. The shock was biphasic with 12 msec duration with the leading edge for second phase

equal to the trailing edge of the first. Computer 2 was used mainly as a recording system, using a pre-set sampling rate. The digitalized data were saved on computer 2. The timing and pacing program was written in C.

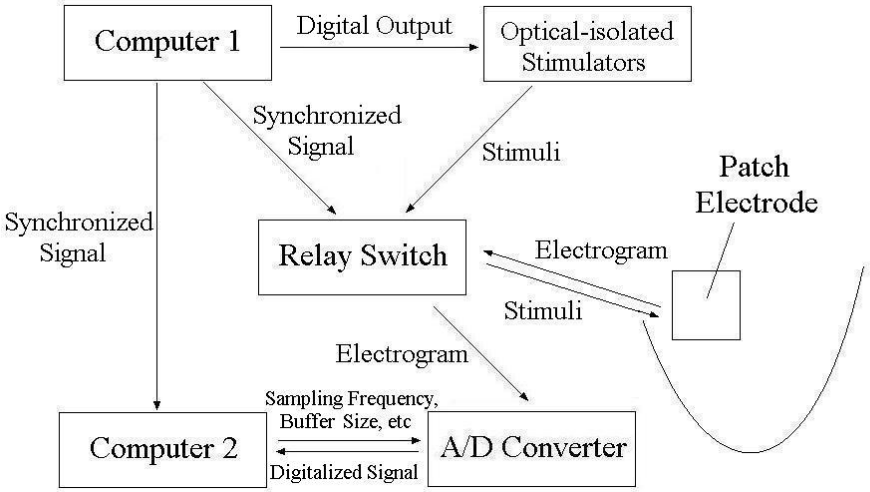

Figure 2.3 Schematic of the experimental setup used to deliver timed stimuli through distributed stimulators in order to modify and entrain activation intervals during VF.

2.4 Data Acquisition

Epicardial electrograms were acquired from the 121-electrode patch (Figure 2.1) by two synchronized, 64-channel, 16-bit analog to digital (A/D) converters (NI 6033E, National Instruments). Thirty-five-second episodes of VF were recorded, which included 5 seconds of stimulation to induce VF, 5 seconds to allow VF to stabilize and 15.2 seconds of pacing to entrain VF. The data were acquired at the rate of 1500 samples per second per channel. The data-acquisition program was written in LABVIEW.

2.5 Pacing Protocol

Spatio-temporal distributed stimuli paced the right ventricle free wall through the 64-stimulation electrodes on the patch (Figure 2.1) with each row of electrodes grouped as one channel of the 8-channel stimulator. The stimulator design is described below. The time interval between stimuli from sequential rows was estimated from the

conduction velocity and the distance between channels. Different values of pacing cycle length were used to determine which pacing cycle lengths resulted in better entrainment. In all trials, each pacing cycle length was repeated for 20 cycles, initial pacing cycle length was 130msec, which was decreased to a minimum cycle length of 60 msec in steps of 10msec. Four (1st, 3rd, 5th, and 7th rows) or eight stimulators were used in experiments.

2.6 Stimulator Design

Eight optically isolated biphasic stimulators were designed and fabricated, each stimulator was addressable via digital inputs and could be independently triggered. The circuit diagram for one of the stimulators is shown in Figure 2.4.

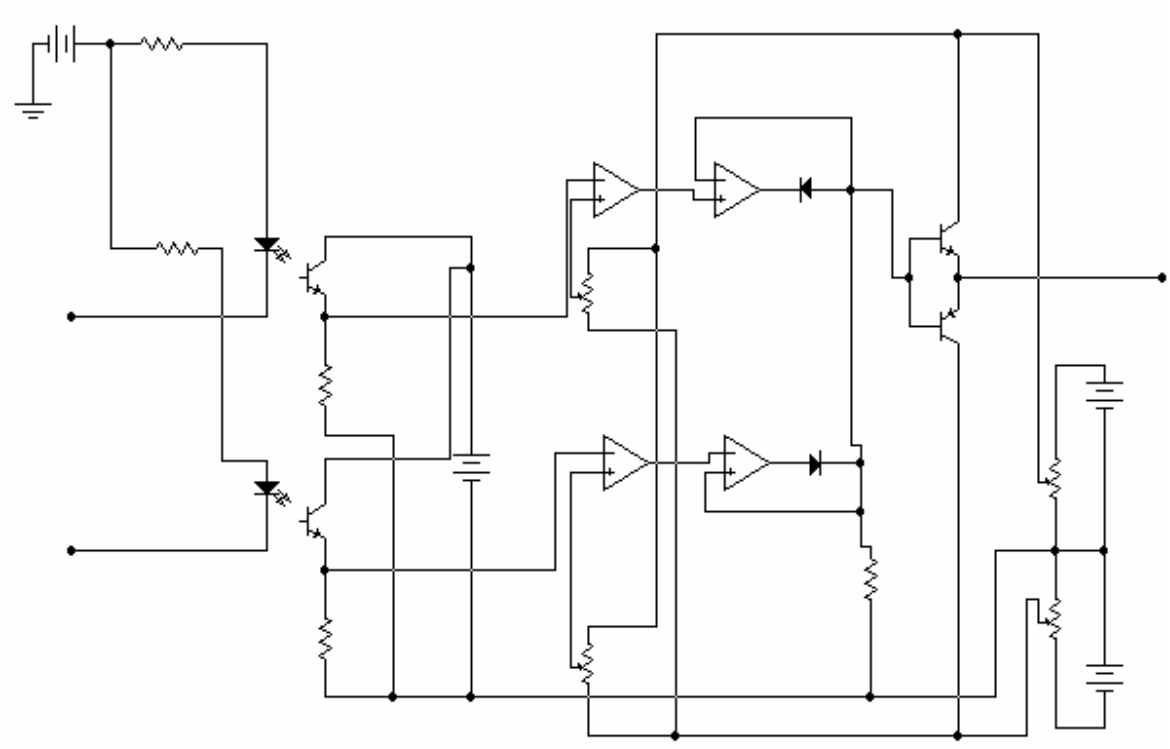

Figure2.4 Circuit diagram of a stimulator used to deliver distributed stimuli. Digital inputs from the computer are optically isolated from the pulse output circuit.

All digital inputs from the timing controller code (running on computer 1) were optically isolated from the pulse generator part of the circuit. Two Pairs of 9V (total 18V)

batteries were used as the power source to drive the coupled power transistors, which provide the current for the stimulator pulses. A custom program, written in C, was used to time digital output on an A/D card (National Instruments PCI 6033E), which delivered TTL pulses to time the sequence of stimulation. The parameters that could be changed were pulse intensity (through potentiometers on the stimulator circuitry), pulse polarity, and duration, as well as interpulse interval and pacing cycle length. The stimulators' output at 100 msec pacing cycle length is shown in Figure 2.5.

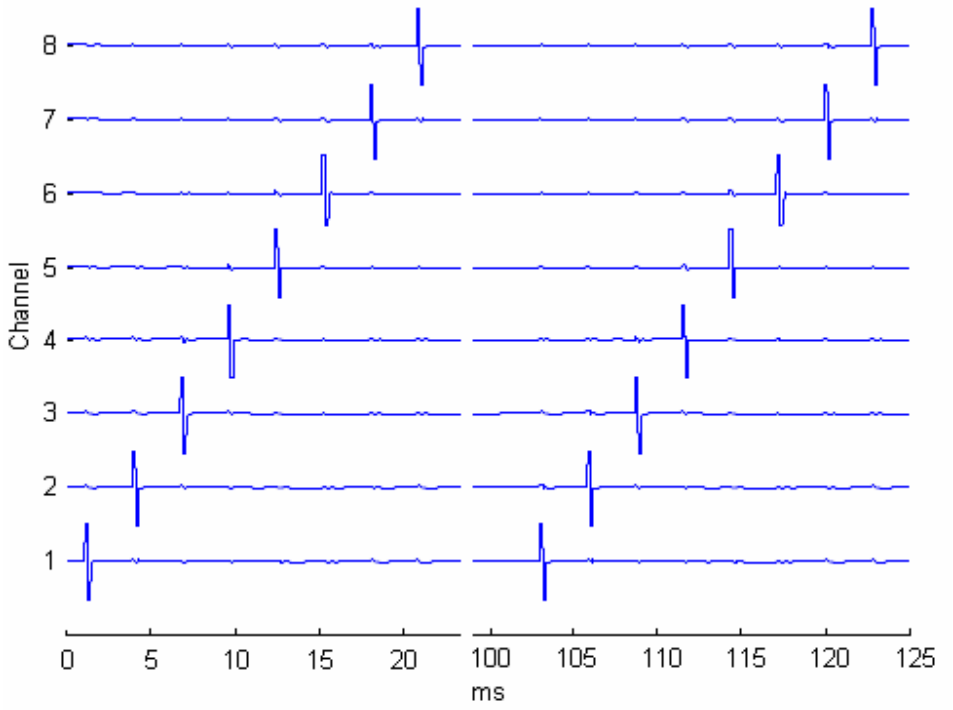

Figure 2.5 The stimulator's output as applied to the epicardium. Shown are two cycles at cycle length of 100 ms. Note that to show two cycles the time interval between is not plotted to scale.

2.7 Data Analysis

The electrograms from 121 channels were visually inspected to eliminate the channels with bad signal quality. The stimulus artifacts were first removed by the use of threshold detection followed by cubic spline interpolation. A low-pass filter at 40Hz was then applied on the stimulus "blanked" electrograms. Filtered signals were re-sampled at 100Hz and the DC component was removed. Time-frequency information was

obtained using smoothed pseudo-Wigner distribution (SPWD) for all the channels. The SPWD at one time step (t_0) is given in equation 2.3.

$$SPWD(f,t_0)=\sum_n h(n)\sum_i w(i)e^{-j2\pi fi}x(i)x(n-i) \qquad Eq.\ 2.3$$

where f is the frequency index, n is the window length, h and w are the time and frequency smoothing windows respectively, and x is the signal segment (10). Blackman and Hanning windows were used for time and frequency smoothing respectively. The real frequency is half of frequency computing using SPWD. A 630 msec time window (63 points) and a 60 msec time step (6 points) were used in computing SPWD. The dominant frequency was determined for each time step in the frequency range from 4Hz to 20Hz.

In order to quantify the spatial similarity, time-varying coherence was computed from pairs of signals. Coherence is a quantitative measure of the similarity between two signals at a specific frequency. The coherence, $C_{xy}(f)$, between two signals x and y is defined in equation 2.4.

$$\left|C_{xy}(f)\right|=\sqrt{\frac{S_{xy}(f)^2}{S_{xx}(f)S_{yy}(f)}} \qquad Eq.\ 2.4$$

where $S_{xy}(f)$ is the cross spectrum of x and y. $S_{xx}(f)$ and $S_{yy}(f)$ are the auto spectra of x and y respectively. An adaptive time coherence algorithm was used to compute coherence changes vs. time as shown in equation 2.5 (9,11). The variables k and f are the time and frequency index respectively. The variables $h_{xy}(k)$ and $h_{yx}(k)$ are the transfer function between x and y with the un-modeled component of signal described as error function which is minimized to search for parameters of h. The variables $h_{xy}(k)$ and $h_{yx}(k)$ are updated at every time step such that the error is minimized. The gains of adaptation are μ_x and μ_y. X and Y are the segments of x and y at time step k with

the length of $2M+1$. The variables $\hat{x}(k)$ and $\hat{y}(k)$ are the estimate of the middle point of X and Y.

$$h_{xy}(0) = h_{yx}(0) = [0 \ldots 0 \quad 1 \quad 0 \ldots 0]^T, \quad filter \quad length: \quad 2M+1$$
$$\hat{y}(k) = h_{xy}{}^T(k)X(k); \qquad \hat{x}(k) = h_{yx}{}^T(k)Y(k)$$
$$h_{xy}(k+1) = h_{xy}(k) + \mu_x(Y(k, M+1) - \hat{y}(k))$$
$$h_{yx}(k+1) = h_{yx}(k) + \mu_y(X(k, M+1) - \hat{x}(k))$$
$$H_{xy}(k+1, f) = DFT[h_{xy}(k+1)]; \qquad H_{yx}(k+1, f) = DFT[h_{yx}(k+1)]$$
$$C_{xy}(k+1, f) = H_{xy}(k+1, f)H_{yx}(k+1, f) \qquad Eq. \ 2.5$$

In equation 2.5 $C_{xy}(k, f)$ is estimate of coherence at time step k. The values of coherence C_{xy} were scaled so that the coherencies computed using the adaptive algorithm were constrained to be between 0 and 1.

Chapter Three: Results

3.1 Results of Numerical Simulation

3.1.1 Simulation of Native VF

Native VF was simulated on the 400X400 matrix for 9 sec of simulation time. We estimated the native VF activation interval (101 msec) by averaging all activation intervals from the 9sec simulation, where the activation interval was defined as the time interval between phase 1 of two consecutive activations. The activation interval varied greatly from time to time. Activation intervals vs. beat number during one simulation unit are plotted in Figure 3.1.

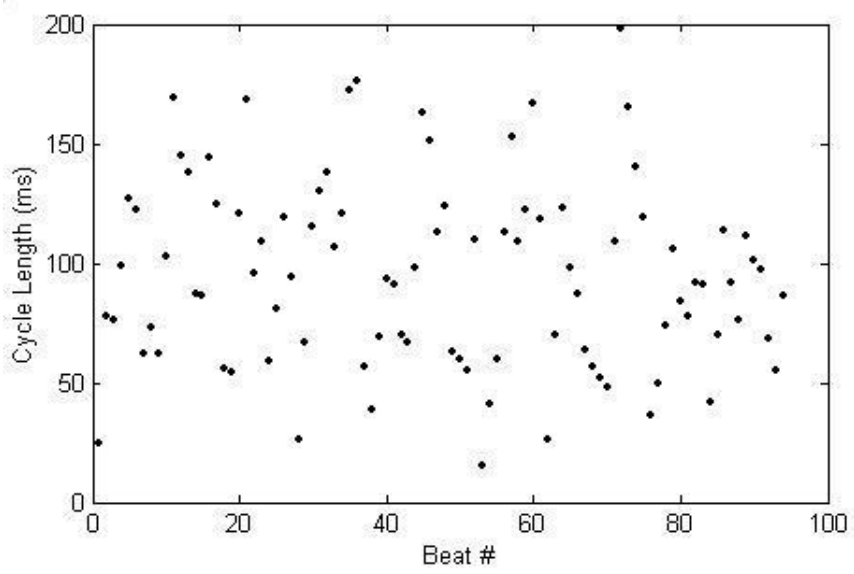

Figure 3.1, Activation intervals vs. beats from 9-Sec simulation

There was no obvious pattern of the change of activation intervals. Conduction velocity was estimated during native VF, to be 2.9 cells (2.9 units in the matrix)/msec (of simulation time).

3.1.2 Entrainment in Numerical Simulation of VF

All simulations of distributed pacing were started from same stage in native VF; after 500 msec (thus ensuring same initial condition), pacing stimuli were initiated from the bottom of the simulation matrix, each row of stimulators fired in a line. The pacing

pattern was similar to what was used in vivo studies, pacing cycle length was started from 130 msec and decreased by 20 msec (a slight difference from the in vivo study) after every 20 cycles and stopped at the cycle length of 50 msec. Simulation was continued for 10 seconds after pacing was stopped. Stimulation was delivered from 16 lines in the matrix; stimuli were delivered in a line of width 3 matrix units (Figure 3.2).

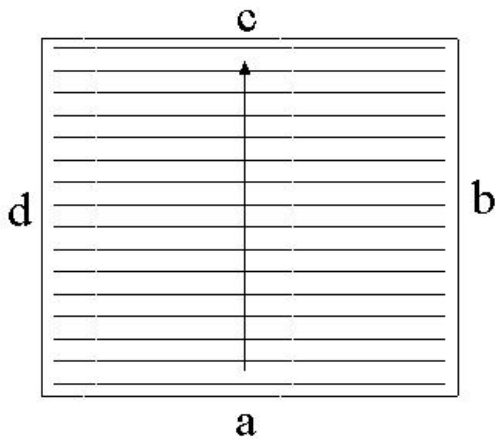

Figure 3.2, The layout of the simulation matrix with the 16 stimulation lines. The arrow indicates the stimulation direction. The sides a and c have no flux boundary conditions. The sides b and d have the circular boundary conditions.

There were 23 matrix units and 8.5 msec time-delay between every stimulated lines based on the estimated conduction velocity.

In the video file, simulation results are displayed as isopotential plots. Blue color corresponds to resting potential (≤-70mv) and red color corresponds to activation potential (≥25mv). All membrane potentials ranged from -80mv to 32mv. The display rate in the video file is one twentieth of the real time; that is the entire 10 seconds simulation is displayed in 200 seconds in the video file.

Simulated VF with stimulation cycle length from 130 msec to 50 msec.

In simulation, capture was defined to be at least three consecutive activations that were initiated by the stimulation in an area no less than 100X100 elements. It could be seen that entrainment were achieved during pacing from animation. Unlike the in vivo experiments, capture could not be sustained for the whole 20 cycles. Entrainment was lost after a couple of cycles or at the time when the pacing cycle length changed. In order to get more quantitative information, activation intervals change vs. time were obtained by differentiation the transmembrane voltage at four random selected elements instead of using time coherence (detail in discussion section).

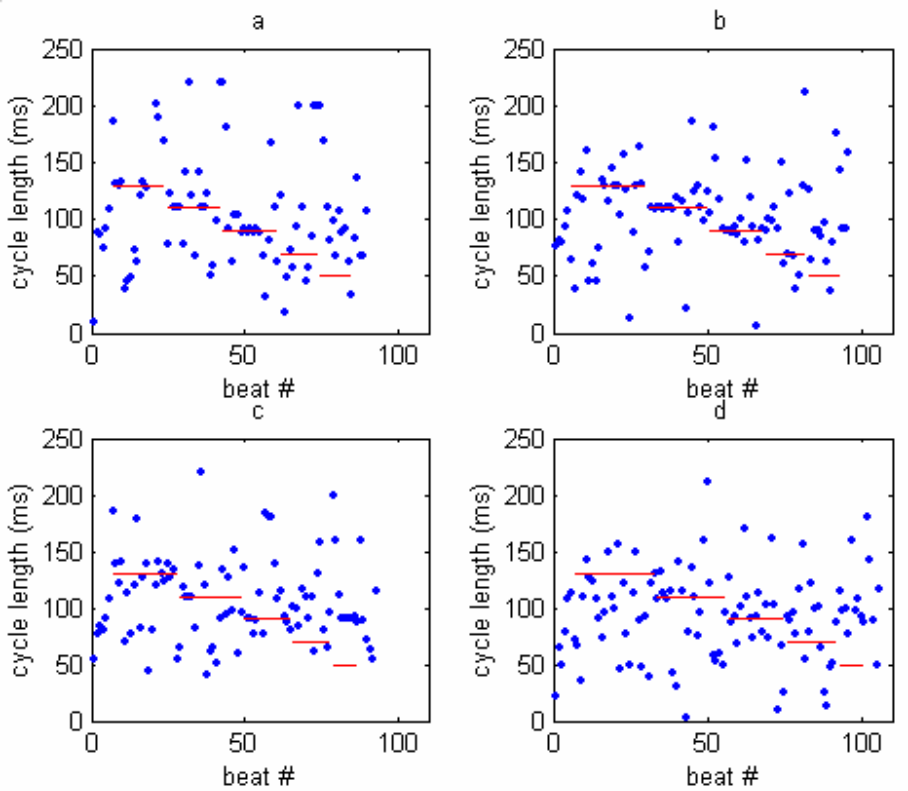

Figure 3.3 The activation interval vs. time (beat #) from 4 simulation matrix units. Blue dots are the activation interval and red lines are the stimulation cycle length at that time.

Figure 3.3 plots the simulation results of the four units respectively, blue dots are the action intervals and the red lines are the pacing cycle length at that time. In all the panels, at least two consecutive activations agree with the pacing rate with the pacing

cycle length of 90 msec. Panel (a) and (b) showed continuous entrainment at pacing cycle lengths of 130 msec, 110 msec and 90 msec, using the criterion that at least two consecutive activation intervals agree with the pacing cycle length. Better entrainment was achieved at pacing cycle lengths of 110 msec and 90 msec; more consecutive activations followed the pacing at these pacing lengths. In panel (c), capture of every other pacing stimulus can be seen at the pacing cycle length of 50 msec, in this case the activation intervals are 100 msec. Panel (d) shows no continuous capture at any pacing cycle length.

3.1.3 Factors Affecting Entrainment Outcome

There are several parameters of the pacing stimuli which affect the results of entrainment, including stimuli strength, stimuli density, pacing cycle length and line stimuli vs. point stimuli.

We found that better entrainment was achieved by increasing the stimuli strength up to a certain limit. In our simulation, if the stimuli strength was around -600mA per matrix unit, the result of pacing would not be improved even if the stimuli strength was increased. Stimuli density also played an important role in pacing; the more dense the stimuli (more close stimulating electrodes), the better the entrainment result was. It is not feasible, however, to increase the stimuli density too much in animal experiments because of such limitations as the size of electrodes and the signal quality. In addition, we also found that, similar to those used by Newton et al (18), line stimuli were better than point stimuli to entrain activations.

3.2 Results of In-vivo Experiments

From data collected during sinus rhythm, we estimated the conduction velocity to be about 1mm/msec in swine. The time interval between channels was calculated from the estimated conduction velocity based on the date collected during VF, of about 0.6mm/msec, and the next line of electrodes was stimulated at the time that the wavefront was expected to arrive at that location. The patch shown in figure 2.1 had

recording electrodes separated by approximately 2 mm in the vertical and 2 mm in the horizontal direction. The vertical spacing between stimulating electrodes was approximately 2mm. Therefore, with conduction velocity of 0.6mm/msec, the interval between stimulator firing was 3.3msec.

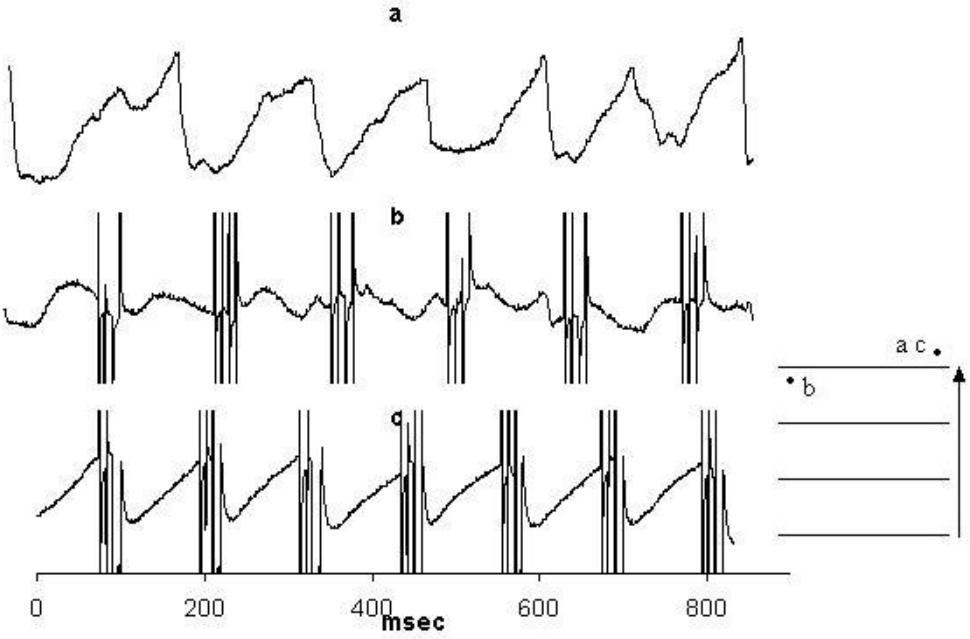

Figure 3.4 Electrograms recorded from an epicardial patch electrode during electrically induced VF in a canine. a. Native VF before inducing stimuli, cycle length varies from 195ms to 110ms. b. Stimuli applied but unable to obtain capture. c. Stimuli applied and good capture with phase locking. Note: The stimuli artifacts were only shown partly. The electrodes position and stimulation direction were shown right.

The native VF cycle length varied greatly from 195msec to 100msec before pacing (Figure 3.4 a). The figure shows example of an electrogram from a VF trial in a dog. During pacing, the tissues under some electrodes showed capture for 7 consecutive cycles (Figure 3.4 c); while some did not (Figure 3.4 b). Panels (a) and (c) were electrograms recorded from the same electrodes at different times. Panel (a) shows considerable variance in the cycle length, which is a feature of native VF. Panel (c) shows the phase locking between activation and the stimuli artifacts; activation occurs after the last stimuli. This recording electrode was located above the last row of

stimulators, therefore, the data in panel c, can be used as evidence of good capture. As shown by the stimulation direction, the cells underneath this electrode should be activated by the activation from the cells excited by the last stimuli, which agrees with the electrogram in panel (c). The electrodes positions are shown in the right side of the Figure 3.4 by dots, also shown is the relative location of stimulating electrodes (the arrow indicates the pacing direction). Although phase locking is a strong proof of capture, it is not feasible to find the exact activation isochronal sequence by differentiation of electrograms because of the unavoidable electrical artifacts.

Time frequency information was obtained by use of SPWD after eliminating the stimuli artifact and low-pass filtering at 40Hz. As stated in the methods section, data were re-sampled at 100Hz. A 630 msec (63 points) window and 60 msec (6 points) time steps were used. From every data window (63 points long), the DC component was removed and zero padding was used to extend data length to 1024 points. A 1024-point Fourier transform was computed and the dominant frequency (rate of activation) was estimated as one half of the frequency of the dominant peak. The frequency doubling occurs because of multiplication during computation of Wigner kernel used in SPWD.

The criterion of successful capture at one electrode that we used was similar to that used by KenKnight (7) which is that the dominant frequency agrees with the stimuli cycle length for at least 3 consecutive pacing cycles. The results from canines for two different pacing protocols are shown in the Figure 3.5 and 3.6; in Figure 3.5 for the VF episode where we used 8 stimulators and in Figure 3.6 for the episode with 4 stimulators. Both Figures show the changes dominant frequency, vs. time, computed using SPWD, at 11 randomly selected electrodes. The asterisks indicate the beginning and the end of the stimulation. The locations of the electrodes are shown in the last panel of each Figure and the lines indicated the positions of stimulator electrodes with the arrow denoting pacing direction. The electrograms showed it was difficult to entrain at the location close to apex and LAD (bottom and right of the patch). Based on this information, we placed the patch close to the base of the heart in swine. We got similar

results in swine except that there were fewer electrograms that showed entrainment at the pacing cycle length of 60 msec (Figure 3.7). As expected, entrainments were improved at the bottom and right of the patch.

The dominant frequency before pacing varied considerably from 6 to 13Hz (Figure 3.5, 3.6, 3.7). During pacing, activations of epicardial cells underneath some electrodes were entrained by the stimuli, that is, the dominant frequencies followed the pacing frequency (reciprocal of pacing cycle length) during all or some cycles.

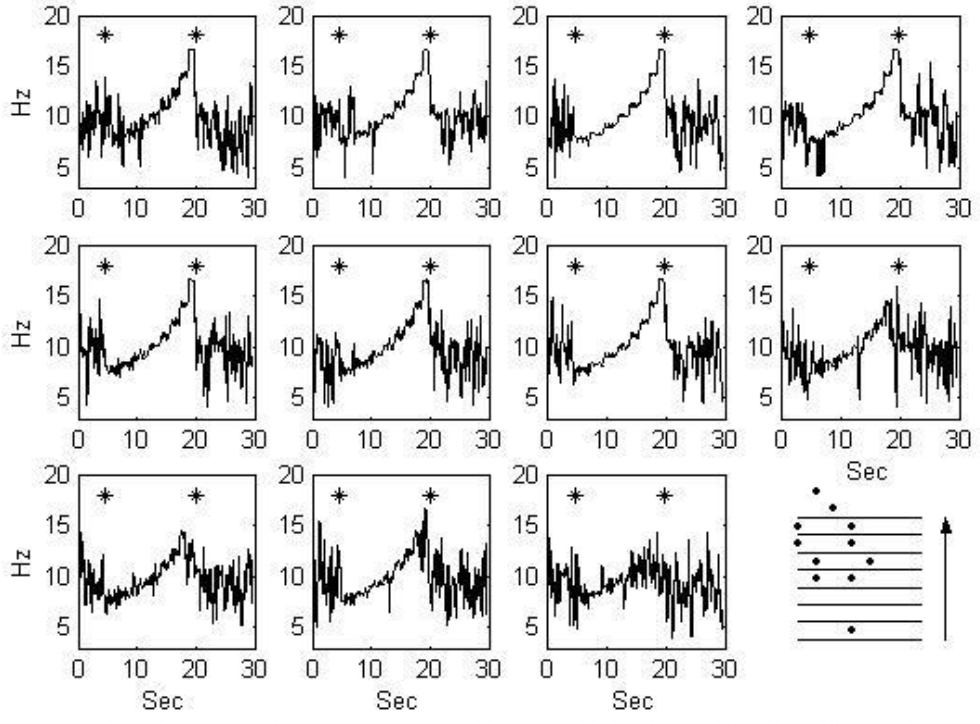

Figure 3.5 Results of time-frequency analysis using SPWD. The first 11 panels showed dominant frequencies change vs. time in random-selected electrodes. The two stars in every panel indicated the start and end point of stimulation respectively. The 11 electrodes positions were shown in the last panel and the stimulator electrodes in the same channel were connected in lines with the arrow indicating the pacing direction. The distributed stimulators were programmed to deliver stimuli in steps of increasing pacing frequencies. The stimulation protocol is reflected in increasing entrained frequencies until the stimulation was stopped. 8 stimulators were used in this trial.

The pacing cycle lengths were started from 130 msec and decreased by 10 msec after every 20 cycles; correspondingly, the dominant frequency of entrained epicardium was expected to change from 7.7Hz to 16.7Hz (as shown in the 3rd panel in the top row of Figure 3.5). All electrograms from the eleven electrodes showed capture at relatively lower pacing frequencies. Loss of capture normally happened at the time when pacing cycle length changed, but capture could be regained after several pacing cycles. Figure 3.5 to 3.7 show that when pacing stopped, the dominant frequencies of all electrodes varied greatly, as during native VF.

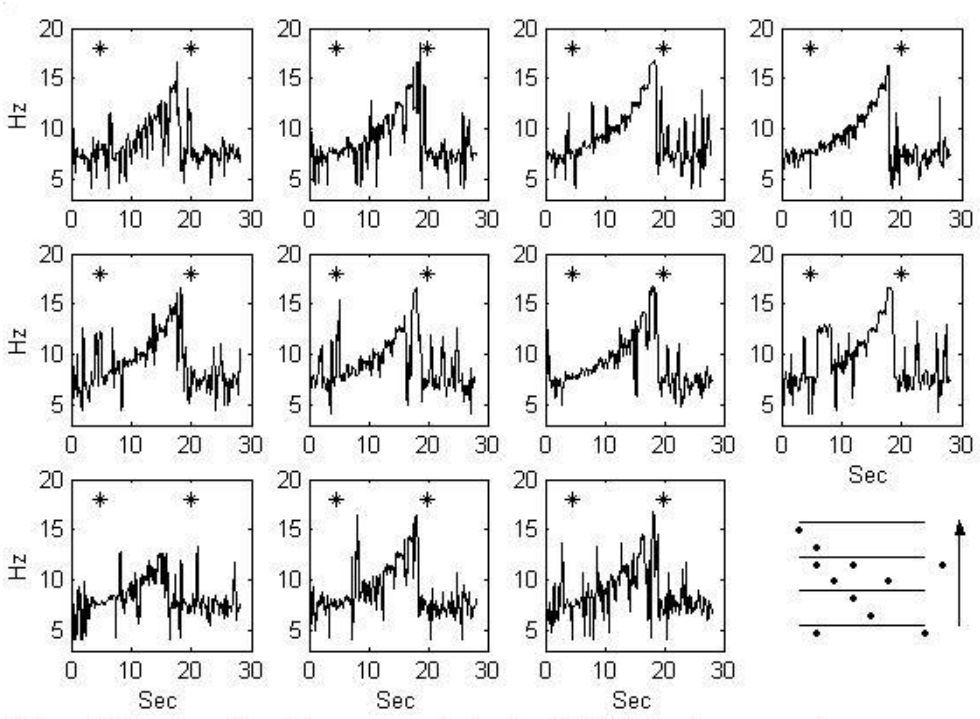

Figure 3.6 Results of time-frequency analysis using SPWD. The layout was the same as figure 3.5 except that 4 stimulators were used in this trial.

We obtained only temporal information about the dominant frequency at any electrode by the use of SPWD. In order to get the uniformity of activation within an area of tissue at different pacing cycle lengths, the dominant frequencies during each pacing cycle length were calculated for all electrodes.

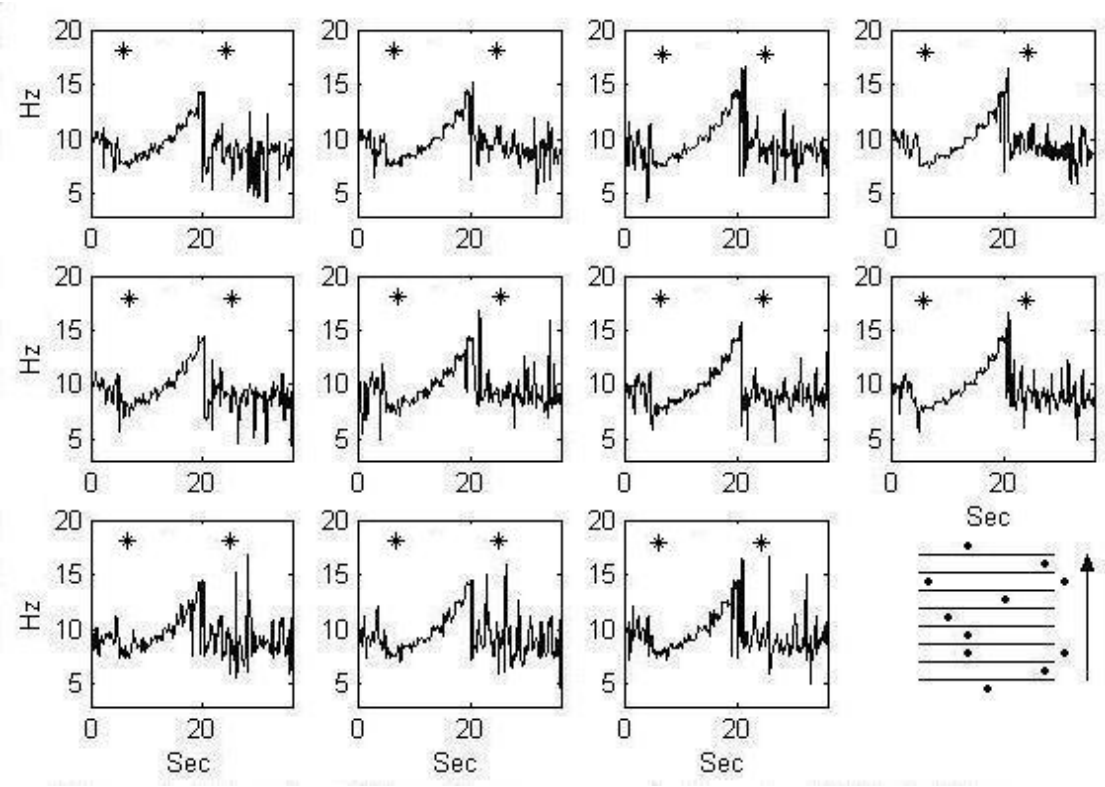

Figure 3.7 Results of time-frequency analysis using SPWD. The layout was the same as figure 3.5 except that data were collected from swine.

The results are given in Figure 3.8 and Figure 3.9 for 8 stimulators and 4 stimulators respectively. All 121 electrodes form an 11 by 11 square matrix. Every element in the matrix represents one electrode and it is shown in black when the dominant frequency at that electrode was within the range given by the pacing frequency±0.2Hz. The pacing cycle lengths are given at the top of every panel.

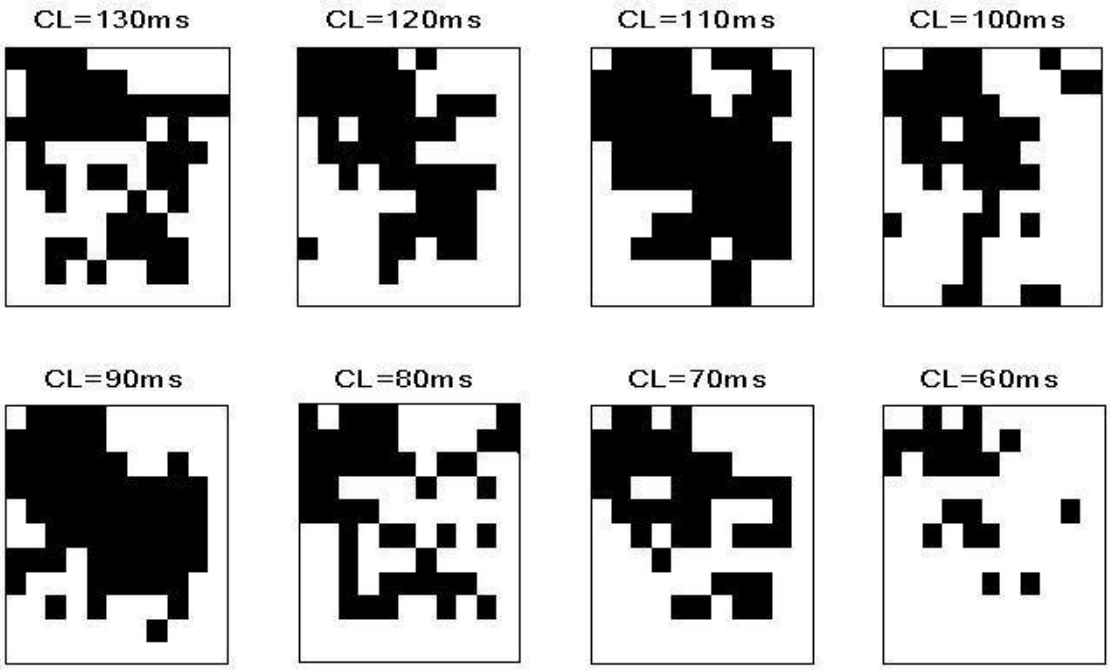

Figure 3.8 Capture at different pacing cycle length with 8 stimulators. The recording electrodes were shown as small squares. The square was black when the electrogram of that electrode had the dominant frequency same to that of the pacing cycle length, otherwise it was white. The pacing cycle lengths were marked at the top of the panel.

Figure (3.5 and 3.6) show that better captures were achieved from cycle lengths of 90 msec, 100 msec and 110 msec than other pacing cycle lengths in canines. Captures were achieved from some electrodes at cycle lengths of 70 msec, 80 msec, 120 msec and 130 msec while only a few electrodes showed captures at cycle lengths of 60 msec.

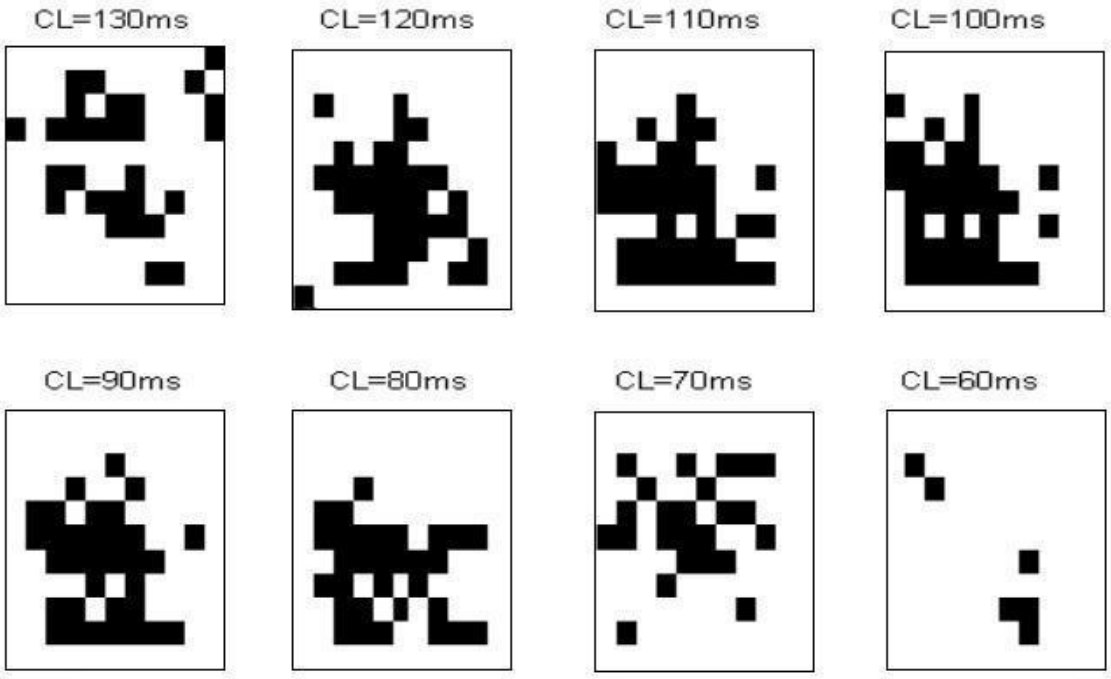

Figure 3.9 Capture at different pacing cycle length with 4 stimulators.

Comparing Figure 3.8 with Figure 3.9, more electrograms showed activation rates matching the pacing frequency with 8 stimulators than 4 stimulators. Also, the electrograms from the

Table 1 Percentage of entrained electrodes at different cycle length from all the trials.

Canine 2-1: the first trial from the second canine

	130m	120m	110m	100m	90ms	80ms	70ms	60ms
Canine 1-1	76.0	73.6	85.1	85.1	66.9	66.1	51.2	47.9
Canine 2-1	53.7	50.4	88.4	89.3	40.5	41.3	44.6	38.0
Canine 2-2	52.9	64.5	86.8	37.2	33.1	33.1	26.4	27.3
Canine 2-3	45.5	94.2	59.5	36.4	42.1	42.1	53.7	52.1
Swine 1-1	74.4	71.9	78.5	71.1	67.8	71.9	53.7	7.4%
Swine 1-2	68.6	83.5	81.0	61.2	58.7	67.8	55.4	19.8
Swine 1-3	68.6	93.4	82.6	66.9	57.0	52.1	31.4	0.8%
Swine 2-1	85.1	89.3	84.3	76.0	67.8	46.3	34.7	23.1
Swine 2-2	94.2	95.9	80.1	66.9	71.1	56.2	50.4	27.3
Swine2-3	90.1	86.0	80.2	76.9	64.5	61.2	43.8	12.4
Swine2-4	86.8	87.6	82.6	74.4	69.4	57.9	39.7	16.5
wine 2-5	86.8	90.9	94.2	83.5	76.0	61.2	34.7	24.0

electrodes away from LAD and apex, where the tissues thickness was thinner, showed better entrainment than others.

A summary of outcome of all the trials from both canines and swine are list in Table 1. The table lists the percentage of entrained channels out of the 121 channels at different cycle lengths. For data shown in this table, a channel was considered to be entrained at a specific cycle length if at least three cycles followed the pacing cycle length.

All the results reported above were obtained using post-experiment analysis. Although we did not use time-coherence computation in real time, such analysis has an advantage that it can be easily implemented in real time. To verify the use of time-coherence for quantifying uniformity of activation due to distributed pacing, time coherencies were calculated from six pairs of electrograms, (a, d), (b, e), (c, f), (d, g), (e, h) and (f, i) (shown in the right top of Figure 3.10 by dots), after eliminating the stimuli artifact.

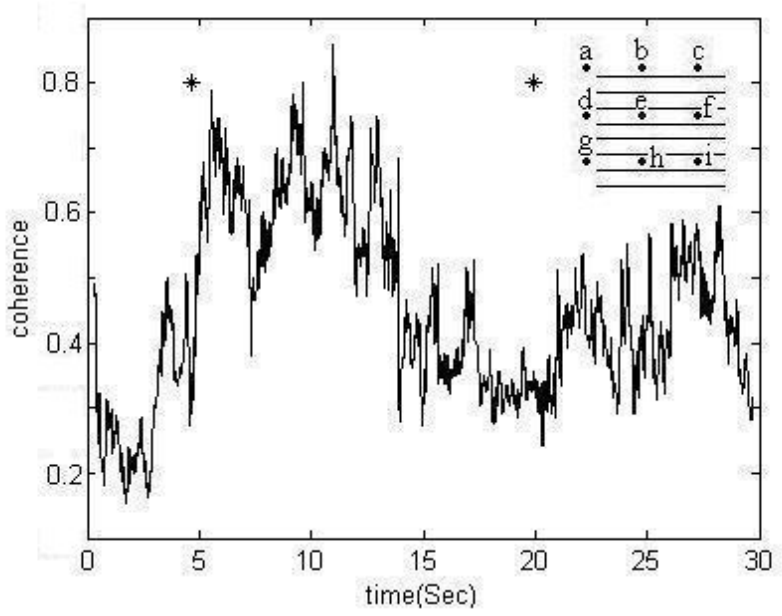

Figure 3.10, Coherence vs. time in canine. The plot here is the average of time-coherences between six pairs of artifact-free electrograms. The six pairs of electrodes are (a, d), (b, e), (c, f), (d, g), (e, h) and (f, i) as shown at top right panel. The asterisks indicate the beginning and end of pacing.

The idea behind using average coherence was that as each coherence indicated the degree of similarity in activation rates between two electrodes, an average of coherencies would then indicate the degree of similarity in activation rates for the entire area that was spanned by these nine electrodes as shown in Figure 3.10. The average of the six time-coherences is plotted in Figure 3.10. The average coherence provided one numerical value at any one time period as the quantitative reference of degree of similarity in activation intervals. The asterisks in the figure indicate the beginning and the end of pacing. During pacing, time-coherences were calculated at the frequency corresponding to the pacing cycle length at that time. Without pacing, time-coherences were calculated at 9Hz, which was the dominant frequency in canines (17). Figure 3.11 is similar to Figure 3.10, except that electrograms were recorded from swine and time-coherences were calculated at 8Hz during intervals of VF without pacing, as the dominant frequency of activation during VF in swine is lower than those in canines.

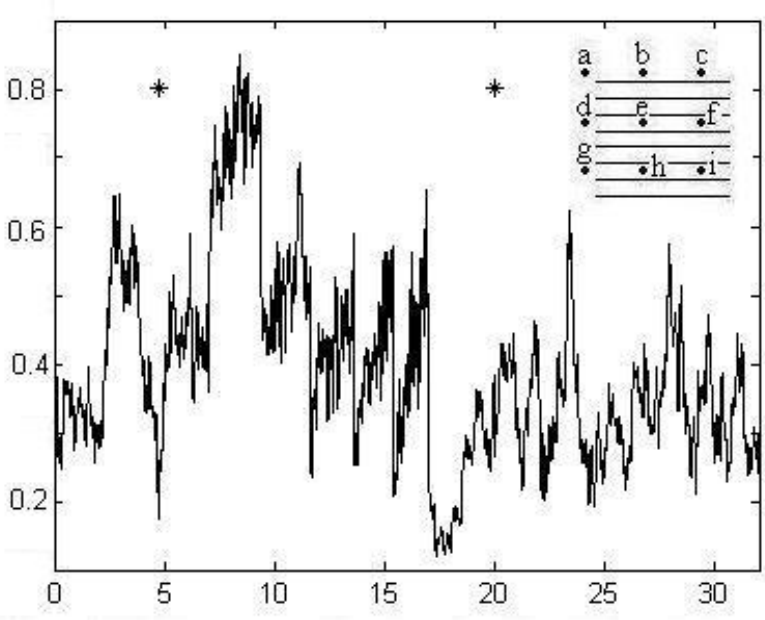

Figure 3.11, Coherence vs. time in swine. The plot here is the average of time-coherences between six pairs of artifact-free electrograms. The six pairs of electrodes are (a, d), (b, e), (c, f), (d, g), (e, h) and (f, i) as shown at top right panel. The asterisks indicate the beginning and end of pacing.

As seen Figure 3.10 and Figure 3.11, coherence increased during pacing and decreased after pacing. The peak of coherence appeared between 8sec and 16sec after initiation of VF, during which time the pacing cycle length was between 120 msec and 90 msec. The coherence peak appears earlier in Figure 3.11 than Figure 3.10. This means that the pacing frequency with best capture in swine is lower than that in canines.

In summary, the main findings from in-vivo experiments were: 1) distributed stimuli could entrain the activations during VF; 2) outcome of entrainment was related to the density of stimuli, pacing cycle length, and the intrinsic properties (thickness) of tissue.

Chapter Four: Discussion

The main findings of the present study were: (1) distributed pacing strength stimuli could entrain activation during VF; (2) the results of entrainment were influenced by pacing cycle length, stimuli density and stimuli strength in addition to tissue properties such as conduction velocity and tissue thickness.

4.1 Entrainment during VF is Possible with Spatio-Distributed Pacing

The results from experimental data analyzed using the SPWD showed capture by the pacing stimuli. Due to the unavoidable electrical stimulus artifacts, a question remains whether the match in frequency was because of the synchronized activation or the stimulus artifacts misled us. We conclude that the results from SPWD were not because of the stimulus artifacts but from real entrainment based on the following four reasons.

1) Before time frequency analysis (SPWD), the stimulus artifacts had been removed by the use of threshold detection followed by cubic spline interpolation. The SPWD algorithm was used on the stimulus artifacts "blanked" signals.
2) The stimuli artifacts were confined in a very short period. With optically isolated ground plus the compensation from the negative part of the biphasic pulse, the capacitor effect of stimulus artifact was reduced substantially. The stimuli duration was 0.9 msec per biphasic pulse. Considering the residual capacitor effect in tissue, the stimuli artifacts were no more than 1.5 msec per pulse. Therefore the electrograms between the stimuli artifacts from two channels were still valuable, although the interval between channels was as short as 6 msec. Even in the shortest pacing cycle length, 60 msec and 8 stimuli per cycle, 80% of the signal was preserved. At longer pacing cycle lengths, over 90% signal was recoverable.
3) Comparing Figure 3.4b with Figure 3.4c, although there were stimuli artifacts, we could tell capture from the phase locking in Figure 3.4c, as could SPWD, while in 3.4b this locking was absent, again picked up by the SPWD.
4) An extension of the above point is that if stimulator artifacts were misleading our analysis, capture would have been observed over all 121 electrodes, which was not the case.

4.2 Stimuli Properties that Affect Entrainment

4.2.1 Stimuli Strength

Previous studies (18) showed current strength would influence capture during VF by pacing from a single line electrode. We got similar results in simulation. We found entrainment efficacy increased when the stimuli strength increased, up to a certain limit (as discussed in the result section). A possible explanation for this observation could be that the activation threshold for relative refractory tissue is higher (19), so increasing the stimuli strength would be able to activate more relative refractory tissue. There was a limitation of stimuli strength of about -600mA; above this limit, the entrainment would not be improved even if we increased the stimuli strength. This observation could be explained with the classic hyperbolic strength-interval curve. Once the stimuli strength approached the asymptote along the curve, the ability to pace would not increase.

4.2.2 Pacing Cycle Length

In contrast with Newton's results (18), we observed the best entrainments were achieved at some pacing cycle lengths in both simulation and in-vivo experiments. In canines, capture efficacy increased when the pacing cycle lengths were 90 msec, 100 msec and 110 msec (Figure 3.8-3.10). Given the dominant frequency of canines is 9Hz (17); the intrinsic VF cycle length is 111 msec. We could see that the pacing cycle lengths that result in better entrainment varied from 80% to 100% of intrinsic VF cycle length. From above, we concluded the capture efficacy would increase when pacing at cycle length was smaller than, but close to, intrinsic VF cycle length. Pacing at cycle length greater than the intrinsic cycle length, native VF wavefronts could enter the region under stimulator electrodes before the stimuli were received. On the other hand, at cycle length much smaller than the intrinsic cycle length, the tissue might still be in absolute refractory period when the stimuli occurred. At cycle length similar to intrinsic cycle length, tissue will be activated by external stimuli before native VF wavefronts arrive at that location and then the successive activations will block the incoming native VF. In this way, the stimuli could push the wavefront moving in the desired direction resulting in entrained uniform activation.

4.2.3 Density of Stimuli

We found that the trials with 8 stimulators achieved better entrainment than the trials with 4 stimulators. Similar results were observed in simulation. Therefore the stimuli density parallel to the stimulation direction influences capture; the denser the stimuli, the better the capture. A likely explanation for this observation is that native VF wavefronts have more chance to enter the entrained area with sparse stimulators.

4.2.4 Line Electrodes vs. Point Electrodes

We tried different types of electrodes in simulation and found that line electrodes achieved better entrainment than point electrodes even at relatively lower stimulation current density. At the same stimulation current density, the line electrode stimulated more area and had more charge than point electrodes. Another reason was that the line electrodes stimulated all the tissue at the same time and therefore avoided the situation of the retrograde activation from the subsequent stimuli activating the tissue between point electrodes.

4.3 Intrinsic Characteristics that May Affect Entrainment

4.3.1 Tissue Thickness

The efficacy of entrainment is also related to the tissue properties underneath stimulators. The electrograms away from the apex and LAD showed better capture than those close to the apex and LAD (Figure 3.5-3.6). In swine, we placed the recording patch away from the apex and LAD, and as expected, we got better entrainment at the bottom and right of the patch (Figure 3.7). The main reason for this difference in entrainment appears to be tissue thickness. Tissue thickness increases near the apex and LAD. Previous studies (20, 21, and 22) suggested that VF pattern is more complex when tissue mass increases. It is possible that more transmural wavlets break up and move towards the surface (23), so the native VF wavefronts are more likely to enter the entrained area with thicker tissue. Another possibility is that the current density decreases when the tissue thickness increases and therefore the efficacy of entrainment decreases.

4.3.2 Spatial Heterogeneity of Action Potential Duration

Pacing stimuli will take effect when the cells are not refractory. Refractory period is correlated with APD. Action potential duration not only varies at different location but also restitutes in time (APD restitution property). We paced all the electrodes at the same rate at one time. It might be possible that cells with short APD were excitable and cells with long APD were still refractory when stimuli started. Another possibility is that native VF activated cells with short APD before pacing stimuli and then those cells would block the pacing stimuli. In both cases, pacing stimuli would lose capture at some part. However, our design was such that after successive cycle of pacing, the APD restitution effects at any location would be eventually minimized.

4.3.3 Conduction Velocity

Conduction velocity is also an intrinsic properties of myocardium that will influence entrainment of VF and it is likely to be more important than others. In our study, we estimated conduction velocity and assumed it as a time-invariant constant through the tissue underneath the patch electrode. In reality, conduction velocity is dispersed spatially; higher in the base, lower in the apex (24). Also conduction velocity exhibits restitution property like APD (28, 29). It is extremely complex, and perhaps unnecessary to accommodate stimuli to the variable conduction velocity at all the electrodes in real time. Our studies showed good entrainment based on the estimated constant conduction velocity. The reason that we could get good results despite ignoring variations in conduction velocity may be that we estimated a relatively fast conduction velocity, and the stimulus at any location arrived before the wavefront caused by the former stimulus arrived at that location. The tissue behind the coming wavefront was still refractory and thus blocked the retrograde activation from the simulating location.

4.3.4 Dominant Frequency

Dominant frequency during VF varies in different species. We observed that the most effective pacing cycle lengths were different for canines and swine and it was very

difficult to entrain activation in swine with too short of a cycle length. A possible explanation for this observation is that the dominant frequency is higher, 9Hz in canines (17), than in swine who have a dominant frequency about 8Hz (23). As discussed above, entrainment is more effective with the pacing cycle length close to the intrinsic cycle length. Therefore the pacing cycle length should be adjusted to the dominant frequency of different species.

4.4 Adaptive Time Coherence Unfit for Simulation

Adaptive time coherence is a very powerful analysis method applied to in-vivo data. We avoided using this method in simulation data because the capture in simulation did not last long enough. By observing the animation of membrane potentials, we noticed that pacing stimuli would usually lose capture after 2 cycles. In other words, it would last no more than 260 msec. In the adaptive time coherence algorithm, we used the window length as long as 630 msec. The coherence, in this situation, was not very meaningful by the averaging effect caused by the long window length since the capture duration was much shorter. Although we could have increased the adaptive gain μ_x and μ_y , and decreased the window length to get better time resolution, the algorithm has a tendency to become unstable at higher gains. Therefore, we cannot apply the adaptive time coherence algorithm to the data where short duration capture is expected, for example, as in our simulation data.

Unlike simulation data, capture was sustained for a relatively longer time once the capture was achieved in in-vivo experiments (Figure 3.5, 3.6, 3.7). Therefore the time coherence algorithm would be an important tool to use, in real time. It could serve as an index of uniformity of activation in studies that are designed using this information to determine opportune time to deliver defibrillation shocks.

4.5 Limitation of the Study

The most valuable information (in terms of activation times) was when stimulus artifacts occurred. Although we minimized the effects of artifacts by using biphasic symmetric stimuli of short duration, the artifacts were unavoidable. The stimuli artifacts

can be reduced by the use of coaxial electrodes, which confined the electrode field in a small area. In Johnson's study (25), recording with coaxial electrodes did reduce stimuli artifacts at the points 4cm away from the coaxial electrodes, but stimuli artifacts were still considerable at distance of 2cm. However coaxial electrodes would not have helped much in our study since the 8 stimulators were uniformly distributed on the 2cm by 2cm patch.

Optical mapping is likely to be the best way to avoid stimulus artifacts since the transmembrane voltage change could be recorded optically. Thus an optical recording system will be 'blind' to the electrical stimuli. Solid support of entrainment could be obtained by recording activation optically during distributed pacing. The drawbacks of optical mapping are 1) impossible use for in-vivo study and 2) no ideal voltage sensitive dye, which would not affect membrane properties. The cell electrophysiology properties are changed by a voltage sensitive dye (27).

4.6 Conclusion

Entrainment of electrical activation is possible during VF. The entrainment outcome is affected by both stimuli properties, like strength, density and pacing cycle length; and intrinsic tissue properties, like dominant frequency and tissue thickness.

References

1. AHA Heart and Stroke Encyclopedia
   http://www.americanheart.org/presenter.jhtml?identifier=4741
2. AHA 2002 Heart and Stroke Statistical Update
   http://www.americanheart.org/downloadable/heart/10461207852142003HDSStatsBook.pdf
3. http://lysine.pharm.utah.edu/netpharm/netpharm_00/druglist/sotalol.htm
4. http://www.wyeth.com/content/ShowFile.asp?id=94
5. Wilson CM, Allen JD, Bridges JB, Adgey AA. Death and damage caused by multiple direct current shocks: studies in an animal model. Eur Heart J 1988 Nov;9(11):1257-65
6. Lammers WJEP, Allessie MA, Rensma PL, Schalij MJ: The use of fibrillation cycle length to determine spatial dispersion in electrophysiologic properties used to characterize the underlying mechanism of fibrillation. N Trends Arrhythmia 1986; 2: 109-112
7. KenKnight BH, Bayly PV, Gerstle RJ, Rollins DL, Wolf PD, Smith WM, Ideker RE: Regional capture of fibrillating ventricular myocardium: Evidence of an excitable gap. Circ Res 1995; 77:849-855.
8. Jones J, Noe W, Tovar O, Lin Y, Hsu W: Can shocks timed to action potentials in low-gradient regions improve both internal and out-of-hospital defibrillation? J Electrocardiol 1998; 31 Suppl: 41-4.
9. Patwardhan A, Moghe S, Wang K, Wright H, Leonelli F: Correlation between defibrillation shock outcome and coherence in electrocardiograms. Pacing Clin Electrophysiol 2001 Sep; 24(9 Pt 1): 1354-62
10. Patwardhan A, Moghe S, Wang K, Leonelli F: Frequency modulation within electrocardiograms during ventricular fibrillation. Am J Physiol Heart Circ Physiol 2000 Aug; 279(2): H825-35
11. Thakor NV, Kong X, Hanley DF: Nonlinear changes in brain's response in theevent of injury as detected by adaptive coherence estimation of evoked potentials. IEEE Trans Biomed Eng. 1995 Jan; 42(1): 42-51.

12. Luo CH, Rudy Y: A model of the ventricular cardiac action potential depolarization, repolarization, and their interaction. Circ Res. 1991 Jun; 68(6): 1501-26.
13. Luo CH, Rudy Y. A dynamic model of the cardiac ventricular action potential. I. Simulations of ionic currents and concentration changes. Circ Res. 1994 Jun; 74(6): 1071-96.
14. Luo CH, Rudy Y. A dynamic model of the cardiac ventricular action potential. II. Afterdepolarizations, triggered activity, and potentiation. Circ Res. 1994 Jun; 74(6): 1097-113.
15. Qu Z, Garfinkel A: An advanced algorithm for solving partial differential equation in cardiac conduction. IEEE Trans Biomed Eng. 1999 Sep; 46(9): 1166-8.
16. Dave JM, Fain ES, Dorian P, and Winkle RA. The relationship between successful defibrillation and delivered energy in open-chest dogs: Reappraisal of “defibrillation threshold” concept. Am Heart J. 1987; 113:77-84.
17. Carlisle EJF, Allen JD, Bailey A, Kernohan AG, Anderson J, and Adgey AAJ. Fourier Analysis of Ventricular Fibrillation and synchronization of DC Countershocks on Defibrillation. J Electrocardiology. 1988; 21:337-43.
18. Newton JC, Huang J, Rogers JM, Rollins DL, Walcott GP, Smith WS, Ideker RE. Pacing during ventricular fibrillation: Factors influencing the ability to capture. J Cardiovasc. Electrophysiol. 2001; 12(1): 76-84
19. Vander AJ, Sherman JH, Luciano DS. Human physiology: the mechanisms of body function. 8th ed., McGraw-Hill, New York, 2001
20. Qu F, Moghe SA, Leonelli FM, Patwardhan AR. Time averaged spatial distribution of epicardial dominant frequencies during ventricular fibrillation. Biomed Sci Instrum 2000;36:379-83
21. Hamzei A, Ohara T, Kim YH, Lee MH, Voroshilovski O, Lin SF, Weiss JN, Chen PS, Karagueuzian HS. The role of approximate entropy in predicting ventricular defibrillation threshold. J Cardiovasc Pharmacol Ther 2002 Jan; 7(1):45-52
22. Ikeda T, Kawase A, Nakazawa K, Ashihara TT, Namba TT, Takahashi TK, Sugi K, Yamaguchi T. Role of structural complexities of septal tissue in maintaining ventricular fibrillation in isolated, perfused canines ventricle. J Cardiovasc Electrophysiol 2001 Jan; 12(1):66-75

23. Qu F. Correlation between dominant frequency and tissue thickness during ventricular fibrillation: experimental and simulation study. MS. thesis 2001 U. of Kentucky.
24. Ujhelyi MR, Sims JJ, Miller AW. Induction of electrical heterogeneity impairs ventricular defibrillation: an effect specific to regional conduction velocity slowing. Circulation 1999 Dec 21-28; 100(25):2534-40
25. Doherty PW, McLaughlin PR, Billingham M, Kernoff R, Goris ML, Harison DC. Cardiac damage produced by direct countershock applied to the heart. Am J Cardiol 1979;43:225-232.
26. Chattipakorn N, KenKnight BH, Rogers JM, Walker RG, Walcott GP, Rollins DL, Smith WM, Ideker RE. Locally propagated activation immediately after internal defibrillation. Circulation 1998 Apr 14;97(14):1401-10.
27. Lee MH, Lin SF, Ohara T, Omichi C, Okuyama Y, Chudin E, Garfinkel A, Weiss JN, Karagueuzian HS, Chen PS. Effects of diacetyl monoxime and cytochalasin D on ventricular fibrillation in swine right ventricles. Am J Physiol Heart Circ Physiol 2001 Jun;280(6):H2689-96
28. Weiss JN, Chen PS, Qu Z, Karagueuzian HS, Lin SF, Garfinkel A. Electrical restitution and cardiac fibrillation. J Cardiovasc Electrophysiol 2002 Mar;13 (3):292-5
29. Banville I, Gray RA. Effect of action potential duration and conduction velocity restitution and their spatial dispersion on alternans and the stability of arrhythmias. J Cardiovasc Electrophysiol 2002 Nov;13 (11):1141-9

Vita

Yiping Gu was born on Aug. 18, 1977 in Shanghai, China. She graduated from Zhejiang University with an undergraduate in Life Science and Biomedical Engineering in 2000.